Transactions on Engineering Sciences vol 3, © 1993 WIT Press, www.witpress.com, ISSN 1743-3533

Axi-symmetric finite element modelling of induction machine end-regions

R. Chedid,[a] A.J. Curley[b]
[a] *Department of Electrical Engineering, American University of Beirut, 850 - 3rd Avenue, New York, NY 10022, USA*
[b] *Department of Aeronautics, Imperial College of Science, Technology and Medicine, Exhibition Road, London SW7 2BT, UK*

ABSTRACT

This paper incorporates an axi-symmetric finite element model to describe the machine end-region magnetic field distribution. The finite element model results can then be used in an harmonic equivalent circuit model to predict the machine performance. An end-region finite element model is developed because it is capable of accurately taking account of the non-linear and eddy current effects in the end-region.

1. INTRODUCTION

An axi-symmetric finite element model will be developed to describe the magnetic field distribution of a squirrel cage induction machine end-region with rotor mounted conducting discs. A further constraint is that the finite element model of the induction machine end-region must also take account of the main air-gap field, which can be calculated using an induction machine equivalent circuit model.

Several axi-symmetric formulations have been proposed. However the one described by Okuda [1], indicates that an axi-symmetric magnetic vector potential formulation has some major advantages over other more commonly used three dimensional formulations.

2. AXI-SYMMETRIC FINITE ELEMENT FORMULATION

An axi-symmetric finite element formulation, and the modifications for stator and rotor laminated regions, with current flowing in the peripheral direction only in the machine end-region, requires the solution of the quasi-static

Maxwell field equations. If we assume that the net current flowing due to eddy currents in the peripheral direction is zero, then a gauge can be chosen in which the divergence of the vector potential **A**, is set to zero.

$$\text{div } \mathbf{A} = 0 \qquad (1)$$

If current density is assumed to have a component in the peripheral direction only, the radial and axial components of vector potential will be zero. To solve Poisson's equation it is possible to utilise Galerkin's method of introducing test functions applied to the following equation. For the end-region problem, the governing equation defined below may be used to define an axi-symmetric formulation.

$$\text{Curl } \upsilon \text{ Curl } \mathbf{A} = \mathbf{J}_s - j\omega\sigma (\mathbf{A} - \mathbf{A}_{mean}) \qquad (2)$$

Equation (1) can be applied to the region defined by the rotor end-ring cross-section shown in Figure 1. This equation can also be applied to the end air-region and laminated regions with the right hand side set to zero. Unfortunately, the realisation of this equation in finite element terms produces an asymmetric matrix which doubles the necessary storage space. It is possible to rearrange equation (2) and integrate over the region using a modified vector potential.

A modified magnetic vector potential defined in equation (3) simplifies the three equations for each node. This modified vector potential is able to reduce the complexity of the integrals and hence reduce computer processing time. The minimisation process also reduces the equations for each node to an elemental system of equations not solving for those nodes on the Dirichlet boundary.

$$\mathbf{A}' = r \, . \, \mathbf{A} \qquad (3)$$

The first order polynomials used to approximate the elemental field variation results in variable flux density in all elements. If the field variation across each finite element is small then it is possible to assume a constant value of reluctivity over each element.

$$\upsilon[S]\{A'\}W = \{J\} + \{C\} \tag{4}$$

$$\text{Where } W = \int_r \int_z \frac{1}{r}\, dr\, dz \tag{5}$$

$\{A'\}$ is the column matrix of modified vector potentials.

$\{J\}$ is the column matrix of source current density

[S] is the stiffness matrix containing the coefficients of the simultaneous equations.

$\{C\}$ is the square matrix of induced current density

The integral W shown in equation (5) can be evaluated using element dimensions. Equation (4) with known boundary conditions represents a complete description for a finite element formulation of the quasi-static electromagnetic problem depicted in Figure 1. Here it is normal practice for the matrices to be assembled by adding the contributions from each element region separately. The assembled operation is facilitated by assuming the current density and reluctivity is constant within each element. After numerical computation of the modified magnetic vector potential matrix in equation (4) the original magnetic vector potential may be calculated by dividing the modified vector potential by its radius.

3. CALCULATION OF END-RING IMPEDANCE

The accurate determination of end-ring resistance is difficult due to the end-ring being joined to a set of rotor bars around its circumference, the distribution of current in the bars being such that some of them are feeding current into the end-ring, while the others are providing the return path. If we assume a sinusoidal current variation in the peripheral direction, and zero current in the radial and axial directions, then end-ring resistance may be determined using the values for nodal magnetic vector potential. The complex current density in the end-ring can be shown to be

$$J_{er} = J_s - j\omega\sigma (A - A_{mean}) \tag{6}$$

The Joule loss in the end-ring in cylindrical coordinates is given by

$$P = \int_r \int_z \int_\theta \frac{|J|^2}{\sigma} r\, dr\, dz\, d\theta \tag{7}$$

Equation (6) may now be substituted into equation (7) and simplified, to obtain the end-ring resistance. The effective end-ring resistance may be derived from the finite element results using

$$R_{er} = \frac{2\pi R_m}{S_{er}\sigma} - \frac{2\pi\omega^2\sigma}{I^2}\left[\frac{1}{6}\int_{S_{er}} |A|^2 \, r\,dr\,dz - |A_d| \cdot S_{er} \cdot R_m\right] \tag{8}$$

where R_m is the mean conductor radius, S_{er} the end-ring cross-sectional area and A_0 is the mean vector potential across the end-ring. The end-ring inductance may be obtained from either total global energy stored or the energy stored in the end-region magnetic field. If we consider the total global energy stored then

$$\frac{L_{er} I^2}{2} = \frac{1}{2}\int_r\int_z\int_\theta \mathbf{J} \cdot \mathbf{A}\, r\,dr\,dz\,d\theta \tag{9}$$

Hence the end-ring inductance in finite element terms becomes

$$L_{er} = \frac{2\pi}{3 S_{er} I}\left[\sum_{j=1}^{N_e} \frac{\Delta_{er}}{3} \sum_{i=1}^{3} A_i'\right] \tag{10}$$

Where A_i' is the modified potential of the ith node defined by equation (3). The inductance of the end-ring may also be obtained by equating the total energy with the energy stored in the magnetic field.

$$\frac{L_{er}^2 I}{2} = \frac{1}{2}\int_r\int_z\int_\theta \mathbf{B} \cdot \mathbf{H}\, .\, r\,dr\,dz\,d\theta \tag{11}$$

Table 1 shows the inductance calculated using Silvester [3] for increasing end-ring radius. Also shown is the inductance calculated with the finite element model using either the J.A or B.H formulations. These results show little difference in the results at small radii, but as the radii is increased the error also increases. Figures 3 and 4 shown the variation of end-ring resistance and reactance against frequency for a coarse and fine mesh, using 609 and 1175 elements respectfully. It is suggested from these results that that at least three layers of elements are required for each skin depth. When the frequency was above about 100 Hz this could no longer be achieved.

4. EQUIVALENT CIRCUIT AND FINITE ELEMENT MACHINE MODEL

The machine will be modelled using a standard harmonic equivalent circuit [2] with the number of branches equal to the number of mmf harmonics included in the model. Accurate values of end-ring resistance and reactance may be obtained from a finite element solution which models the geometry, position and material of the machine end-region.

The problem is solved iteratively with the end-ring rotor current being recalculated from the equivalent circuit model. When the equivalent circuit end-ring current has converged, the torque, input current and power may be calculated, using the equivalent circuit model developed in the previous section. The predicted machine performance at this operating speed are then stored and the next operating speed is considered.

5. 5.5 kW MACHINE PERFORMANCE RESULTS

The 5.5 kW machine was a standard three phase 2-pole machine with rated current and voltage of 11.2 A and 415 V respectively. Figures 4 and 5 show the input current and torque for the complete speed range, and shows good agreement except at low speed. This was thought to be due to iron losses or inter-bar currents. It is also difficult to predict temperature variations inside the machine, which are increasingly difficult to model at low speeds.

6. CONCLUSION

The end-region finite element model was capable of taking into account the non-linear and eddy current effects in a standard induction machine. The validity of the finite element model was confirmed with a comparison with the experimental characteristics of a 5.5 kW machine. This model could be employed in conjunction with a two dimensional machine model of the stator and rotor, accurately predicting changes in the machine performance due to design changes.

REFERENCES

1. Okuda, H. :'Finite element solutions of travelling wave magnetic field and eddy-currents', J. Inst. Electr. Eng. (Japan), 1976, Vol 96, No. 4, pp 75-82.
2. Smith, A., Chan, E. and Curley, A. : 'Performance of Induction motors with shaft mounted discs', ICEM, Manchester, September, 1992.
3. Silvester, P. 'Modern electromagnetic fields', Prentice Hall, London, 1968.

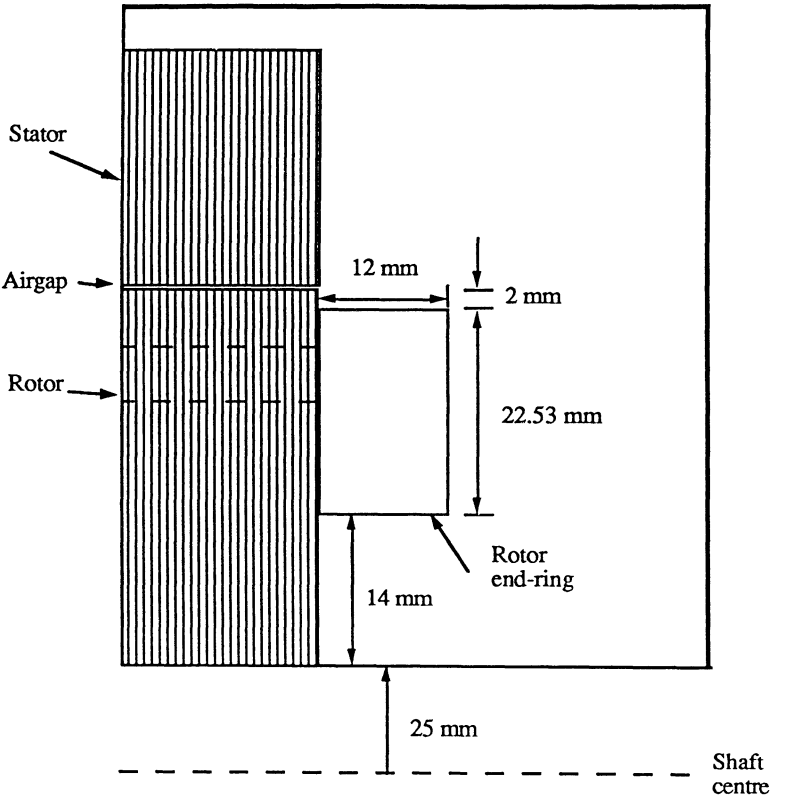

Figure 1 : Induction machine end-ring finite element model

Mean end-ring radius (m)	Inductance calculated using Silvester	Inductance calculated using **J. A**	Inductance calculated using **B.H**
0.035 m	1.648 E-7 H	1.679 E-7 H	1.672 E-7 H
0.135 m	8.65 E-7 H	8.867 E-7 H	8.823 E-7 H
0.535 m	4.35 E-7 H	4.569 E-7 H	4.524 E-7 H
1.035 m	9.28 E-7 H	9.8411 E-7 H	9.744 E-7 H
5.035 m	55.1 E-7 H	61.2 E-7 H	60.059 E-7 H

Table 1. : End-ring inductance results

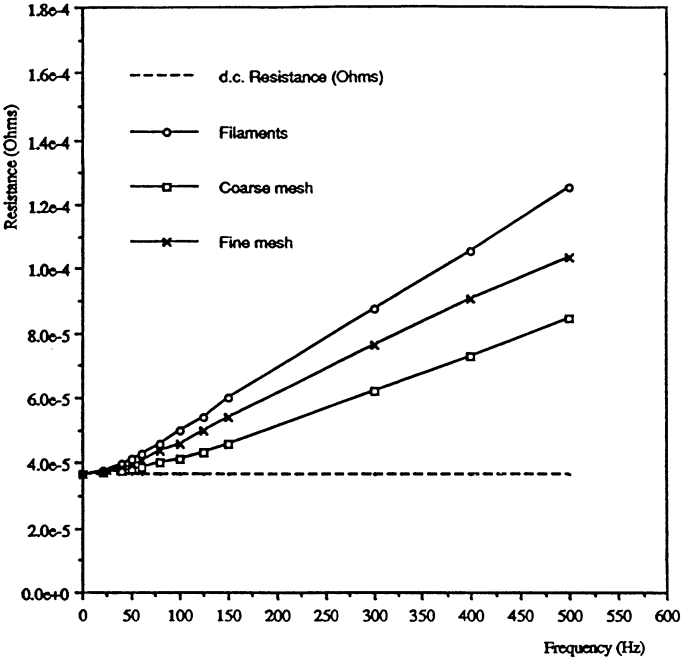

Figure 2 : Graph of end-ring resistance against frequency

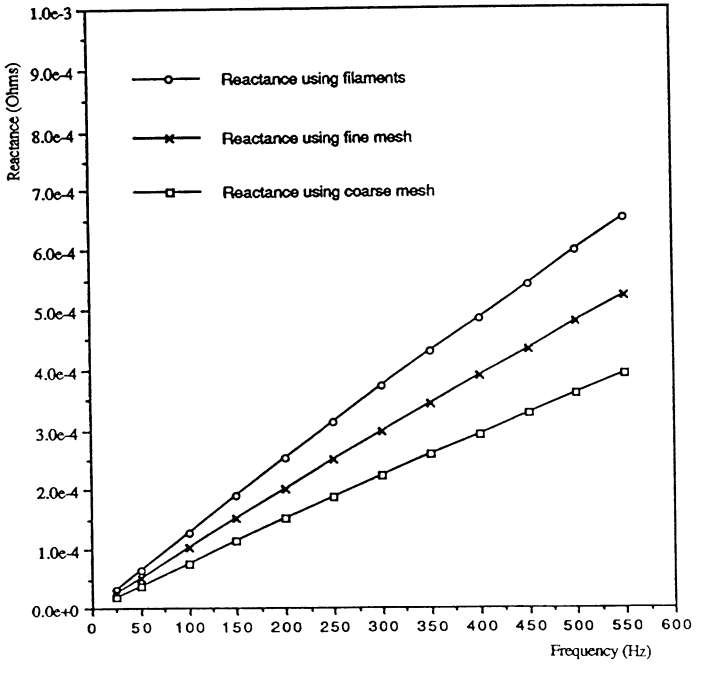

Figure 3 Graph of end-ring reactance against frequency

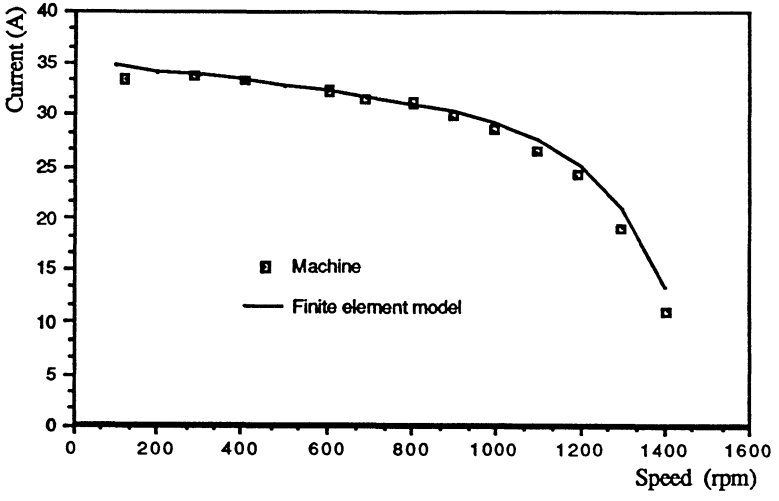

Figure 4 Graph of current against speed

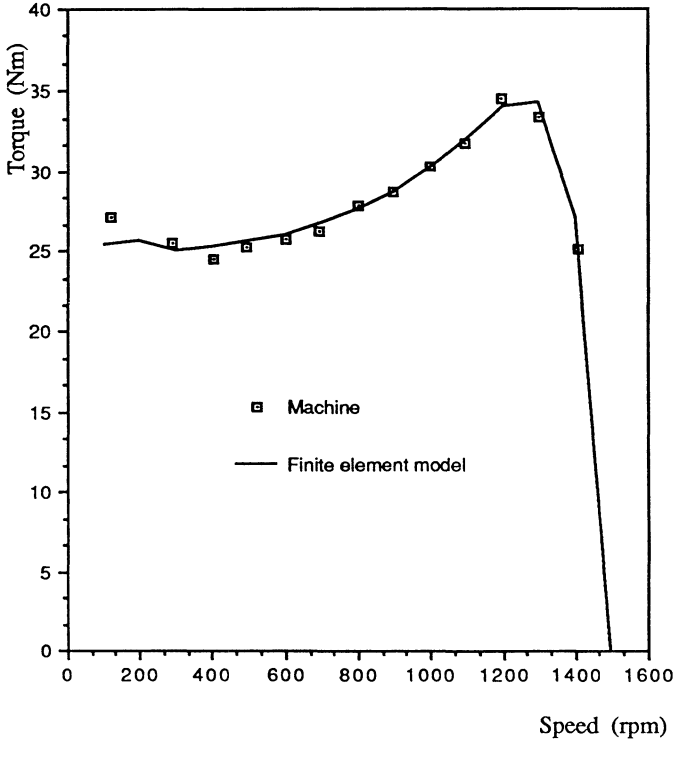

Figure 5 Graph of torque against speed